Supporting Information

Long-Range Spin-Selective Transport in Chiral Metal-Organic Crystals with Temperature-Activated Magnetization

Amit Kumar Mondal,[1#] Noam Brown,[2,3#] Suryakant Mishra,[1] Pandeeswar Makam,[2] Dahvyd Wing,[6] Sharon Gilead,[2] Yarden Wiesenfeld,[4] Gregory Leitus,[5] Linda J. W. Shimon,[5] Raanan Carmieli,[5] David Ehre,[6] Grzegorz Kamieniarz,[6,7] Jonas Fransson,[8] Oded Hod,[3*] Leeor Kronik,[6*] Ehud Gazit,[2*] and Ron Naaman[1*]

[1]Department of Chemical and Biological Physics, Weizmann Institute of Science, Rehovot 76100, Israel.

[2]School of Molecular Cell Biology and Biotechnology, George S. Wise Faculty of Life Sciences, Tel Aviv University, Tel Aviv 6997801, Israel.

[3]Department of Physical Chemistry, School of Chemistry, Raymond and Beverly Sackler Faculty of Exact Sciences, Tel Aviv University, Tel Aviv 6997801, Israel.

[4]Department of Chemistry, University of Pennsylvania, Philadelphia, Pennsylvania 19104-6323, USA.

[5]Department of Chemical Research Support, Weizmann Institute of Science, Rehovot 76100, Israel.

[6]Department of Materials and Interfaces, Weizmann Institute of Science, Rehovot 76100, Israel.

[7]Faculty of Physics, A. Mickiewicz University, 61-614 Poznań, Poland

[8]Department of Physics and Astronomy, Uppsala University, Uppsala, Sweden

* Corresponding authors. Email: O.H.: odedhod@tauex.tau.ac.il, L.K.: Leeor.Kronik@weizmann.ac.il, E.G.: ehudga@tauex.tau.ac.il, R.N.: ron.naaman@weizmann.ac.il

# These authors contributed equally to this work.

Table S1: Crystallographic data

Compound	**L-Phe-Cu**	**D-Phe-Cu**	**L-F_5Phe-Cu**	**D-F_5Phe-Cu**
CCDC	1871975	1871971	1871972	1871973
Diffractometer	ESRF ID23-1	Bruker KappaApexII	Rigaku XtaLabPro	Rigaku XtaLabPro
Empirical formula	$C_{18}H_{20}CuN_2O_4$	$C_{18}H_{20}CuN_2O_4$	$C_{18}H_{14}CuF_{10}N_2O_6$	$C_{18}H_{14}CuF_{10}N_2O_6$
Formula weight (g/mol)	391.90	391.90	607.85	607.85
Crystal description	Blue plate	Blue plate	Blue plate	Blue plate
Temperature (K)	100	100	100	100
Wavelength (Å)	0.70	0.71073	0.71073	0.71073
Crystal system	Monoclinic	Monoclinic	Triclinic	Triclinic
Space group	*$P2_1$*	*$P2_1$*	*P1*	*P1*
a (Å)	9.4800(19)	9.4540(18)	5.56137(13)	5.55855(12)
b (Å)	5.1500(10)	5.1508(10)	7.00144(18)	7.00343(15)
c (Å)	16.670(3)	16.662(3)	13.8993(3)	13.8779(3)
α (°)	90	90	88.590(2)	88.5272(19)
β (°)	98.93(3)	99.199(6)	82.4451(19)	82.5082(19)
γ (°)	90	90	73.562(2)	73.5373(19)
Volume ($Å^3$)	804.0(3)	801.0(3)	514.53(2)	513.64(2)
Z	2	2	1	1
Density calculated (mg/m^3)	1.619	1.625	1.962	1.965
Absorption coefficient (mm^{-1})	1.385	1.391	1.194	1.196
F(000)	406	406.0	303	303
Crystal size (mm)	0.15x0.10x0.01	0.12x0.10x0.002	0.112x0.097x0.03	0.220x0.220x0.050
Theta range for data collection (°)	1.218 to 31.926	2.182 to 26.365	3.853 to 30.630	3.854 to 33.480
Reflections collected (unique)	9071(5472)	8796(3281)	20203(5323)	26978(6968)
R int	0.0435	0.0753	0.0351	0.0379
Completeness (%)	95.3	99.7	89.7	99.7
Data\restraints\ parameters	5472/1/242	3281/19/239	5323/3/343	6968/3/338
Goodness-of-fit on F^2	1.105	0.976	1.008	1.024
Final R [I>2σ(I)]	R1=0.0462, wR2=0.1234	R1=0.0505, wR2=0.0819	R1=0.0231, wR2=0.0569	R1=0.0298, wR2=0.0722
R (all data)	R1=0.0475, wR2=0.1256	R1=0.0814 wR2=0.0908	R1=0.0239, wR2=0.0573	R1=0.0313, wR2=0.0729

Largest diff. peak and hole (e· Å^{-3})	1.416 and -0.548	0.648 and -0.783	0.368 and -0.279	0.535 and -0.541

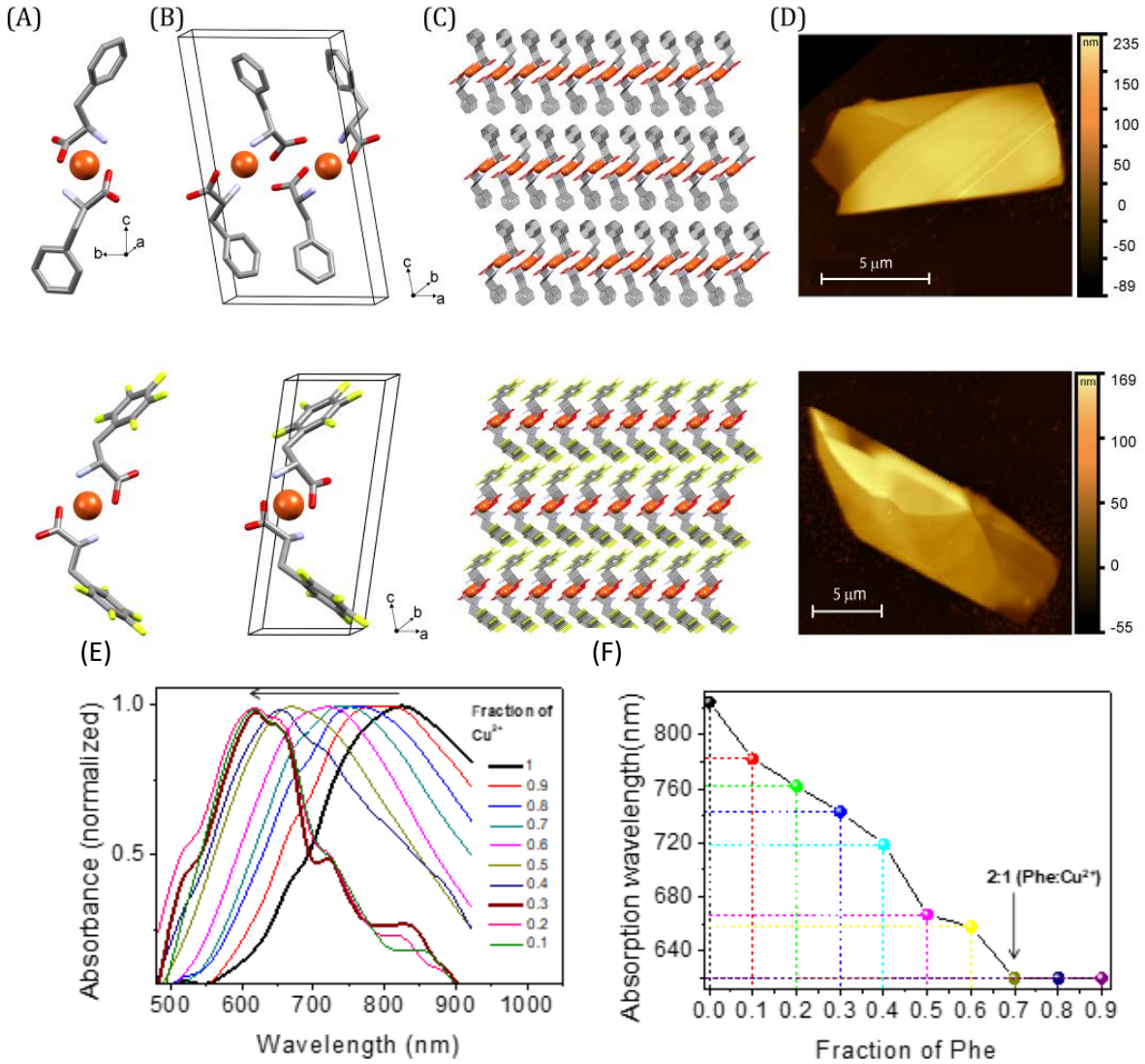

Figure S1: Structure of the D-Phe-Cu (top row) and D-F$_5$Phe-Cu (middle row) crystals. **(A)** Minimal asymmetric unit. **(B)** Unit-cell. **(C)** High-order assembly of the crystal lattice. **(D)** AFM topography image. (**E**) UV-visible absorption spectra at different fractions of Cu^{2+} to Phe. (**F**) The plot of change in absorption wavelength (nm) as a function of the fraction of Phe. The inflection point at a 0.7 Phe fraction, corresponding to a 2:1 (Phe: Cu^{2+}) stoichiometry.

To verify the properties of the coordination complex, the interaction of Phe with Cu^{2+} ions were thoroughly examined by recording UV–Visible absorption spectra at the different stoichiometric ratio of Cu^{2+} to Phe (by keeping the total concentration ([Phe+Cu^{2+}] = 1 mM constant). The $CuCl_2$ (or Cu^{2+} ions) aqueous solution displayed a broad d-d transition absorption band centered at 825 nm (Figure S1E). However, the sequential increase of Phe fraction (or decrease of Cu^{2+} fraction) resulted in a significant blue shift (825 nm to 620 nm) suggesting the

strong carboxylate and amine donor on Phe molecules binding to the Cu^{2+} ions. The plot generated at absorption maxima *versus* the fraction of Phe (Figure S1F) clearly displayed a saturation absorption maximum at 620 nm with an inflection point at a 0.7 Phe fraction, corresponding to a 2:1 (Phe: Cu^{2+}) binding stoichiometry. The observed higher energy band at 620 nm assigned to the $t_{2g} \rightarrow e_g$ transition, specific for octahedral copper complexes with tetragonal distortion owing to the Jahn–Teller effect and the 2:1 (Phe: Cu^{2+}) stoichiometry signifying the optimal ratio for stable complex formation.

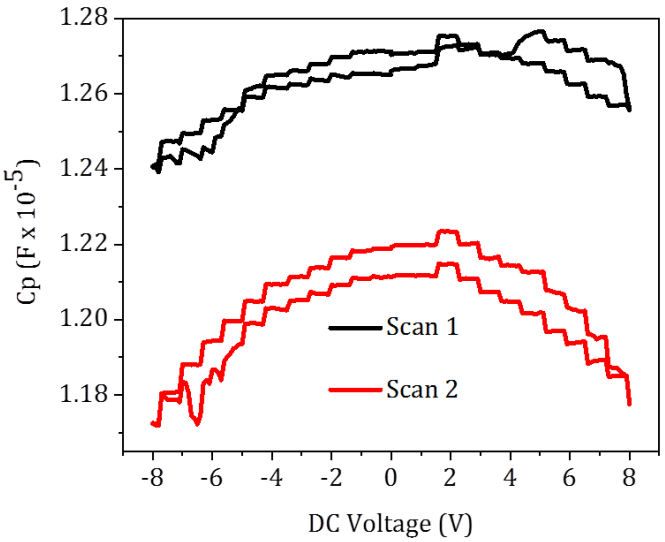

Figure S2: Ferroelectric measurements. Measurement of the capacitance response as a function of voltage for the L-Phe-Cu crystal in 30 K.

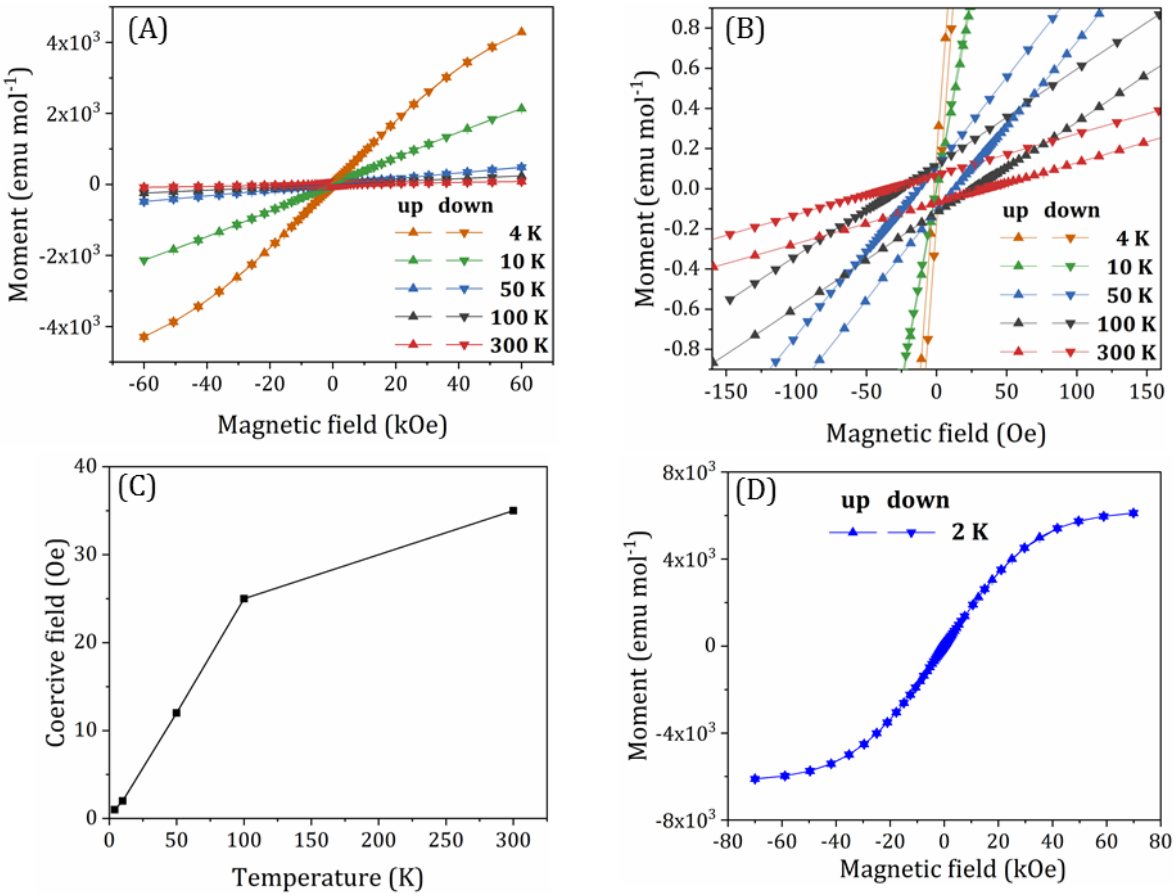

Figure S3: Magnetic properties of L-Phe-Cu crystal powder. (A) Full-spectrum of magnetic moment *vs.* applied field of L-Phe-Cu crystal powder. **(B)** Low-field region of the magnetic moment dependence on the applied magnetic field. **(C)** Coercive field dependence on temperature. Please note that below 5K, the coactivity measured is below the accuracy of the device. **(D)** Magnetic moment *vs.* applied field plot at low temperature (2K) and highest available field (7 Tesla).

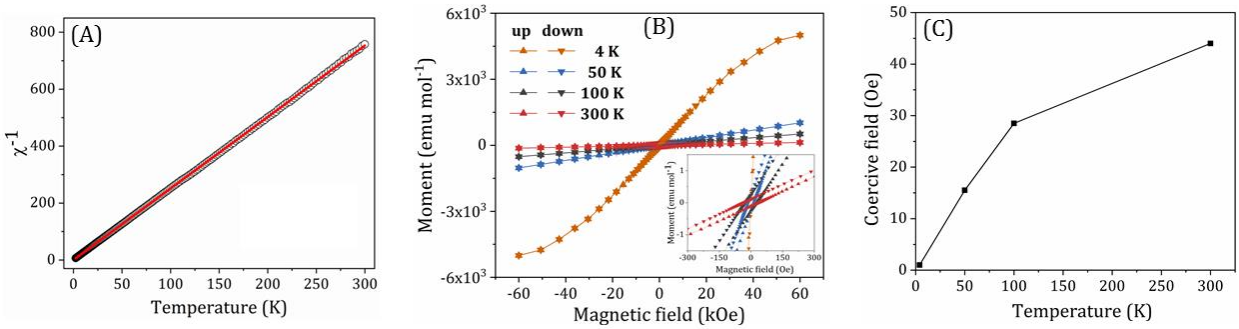

Figure S4: (A) Curie-Weiss fitting of L-Phe-Cu crystal powder in the 2 < T < 300 K temperature region measured at 1000 Oe magnetic field. **(B)** Full-spectrum of magnetic moment *vs.* applied field of D-Phe-Cu crystal powder. Inset: Low-field region of the magnetic moment dependence on the applied magnetic field. **(C)** Coercive field dependence on temperature in the case of D-Phe-Cu crystals.

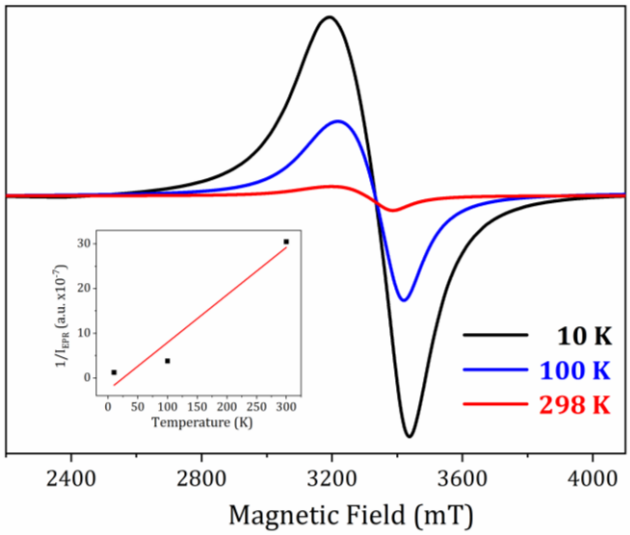

Figure S5: X-band EPR spectra of L-Phe-Cu crystal powder at different temperatures. Inset: inverse of the EPR integral intensity.

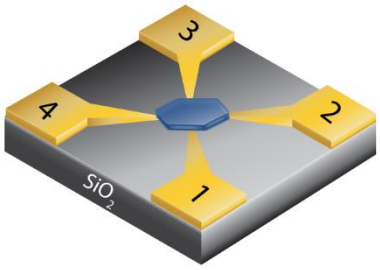

Figure S6: The four contact devices.

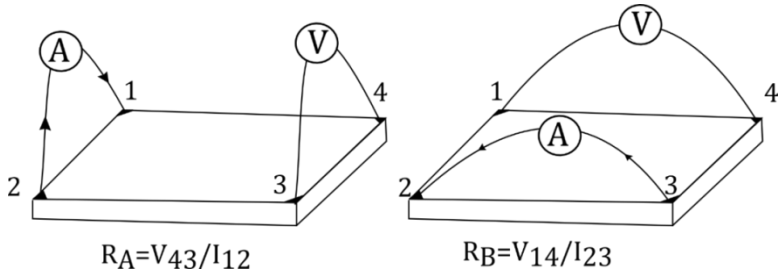

Figure S7: The four contact connection schemes.

Note: The value of R_A and R_B is the average of 100 measurements at each temperature point.

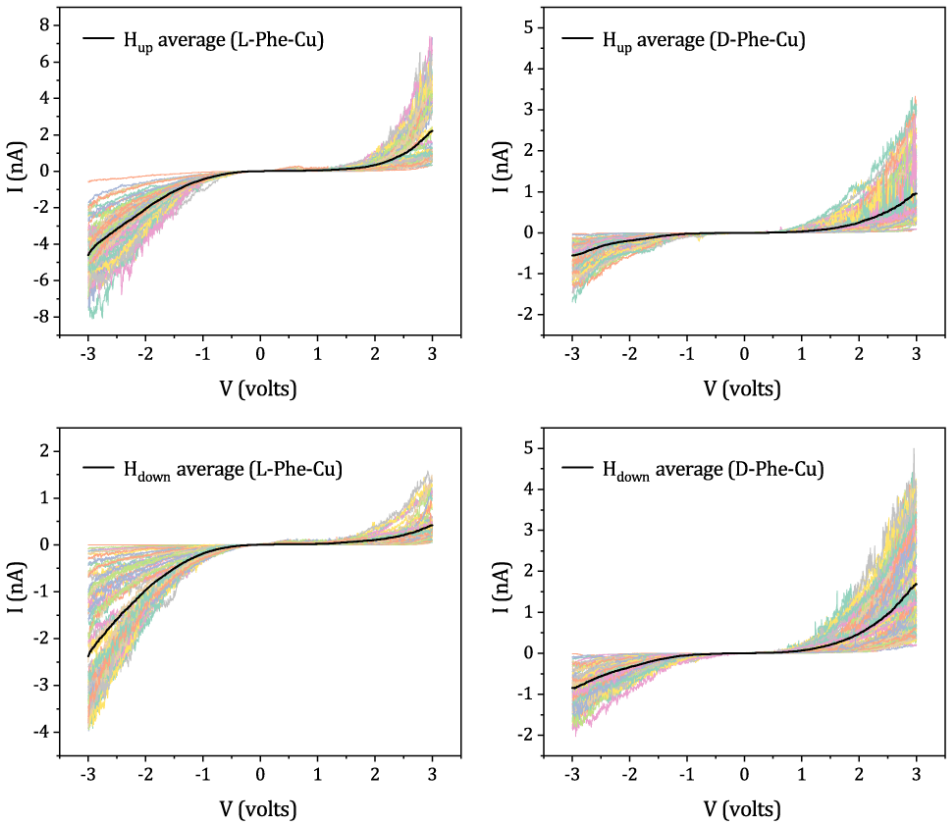

Figure S8: Spin-selective conduction of D/L-Phe-Cu with up/down the external magnetic field. Each line color represents one measurement. Black line represents the average value.

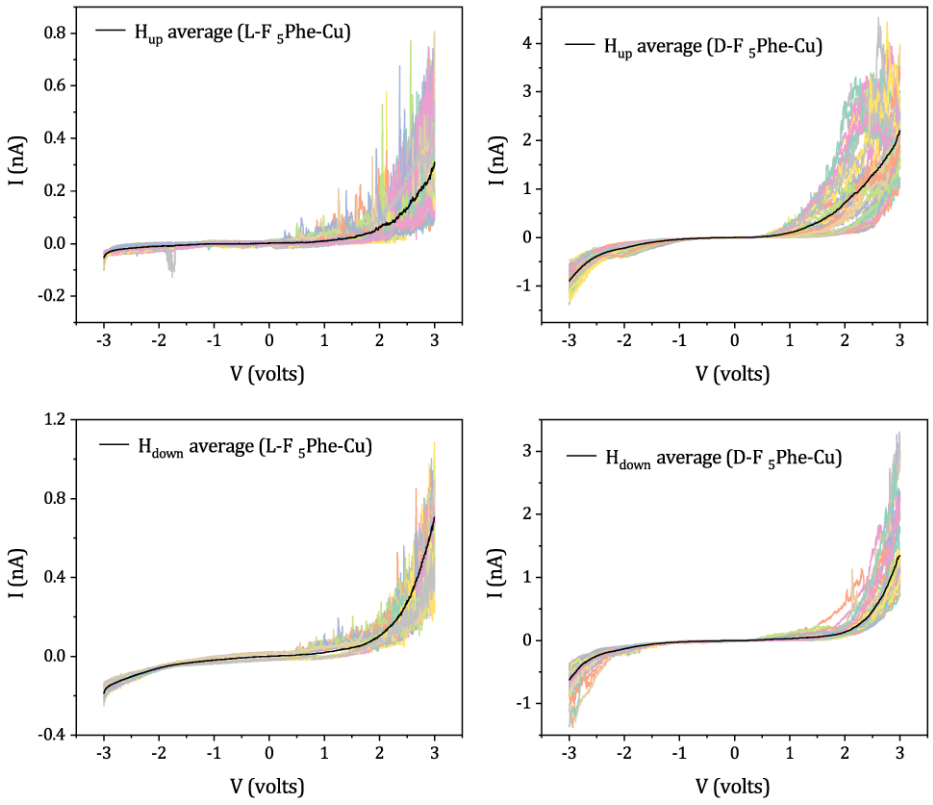

Figure S9: Spin-selective conduction of D/L-F$_5$Phe-Cu with up/down external magnetic field. Each line color represents one measurement. The black line represents the average value.

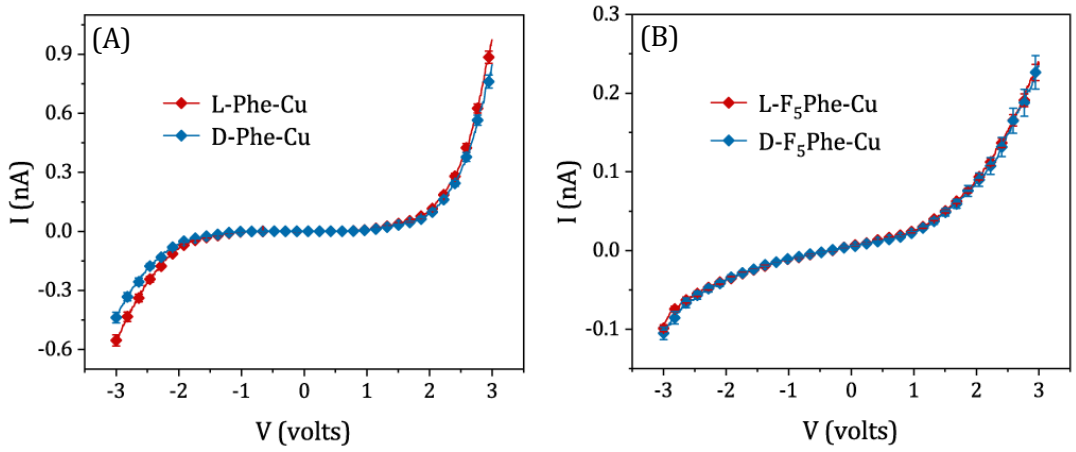

Figure S10: Conduction of D/L-Phe-Cu (A) and D/L-F_5Phe-Cu (B) without an external magnetic field.

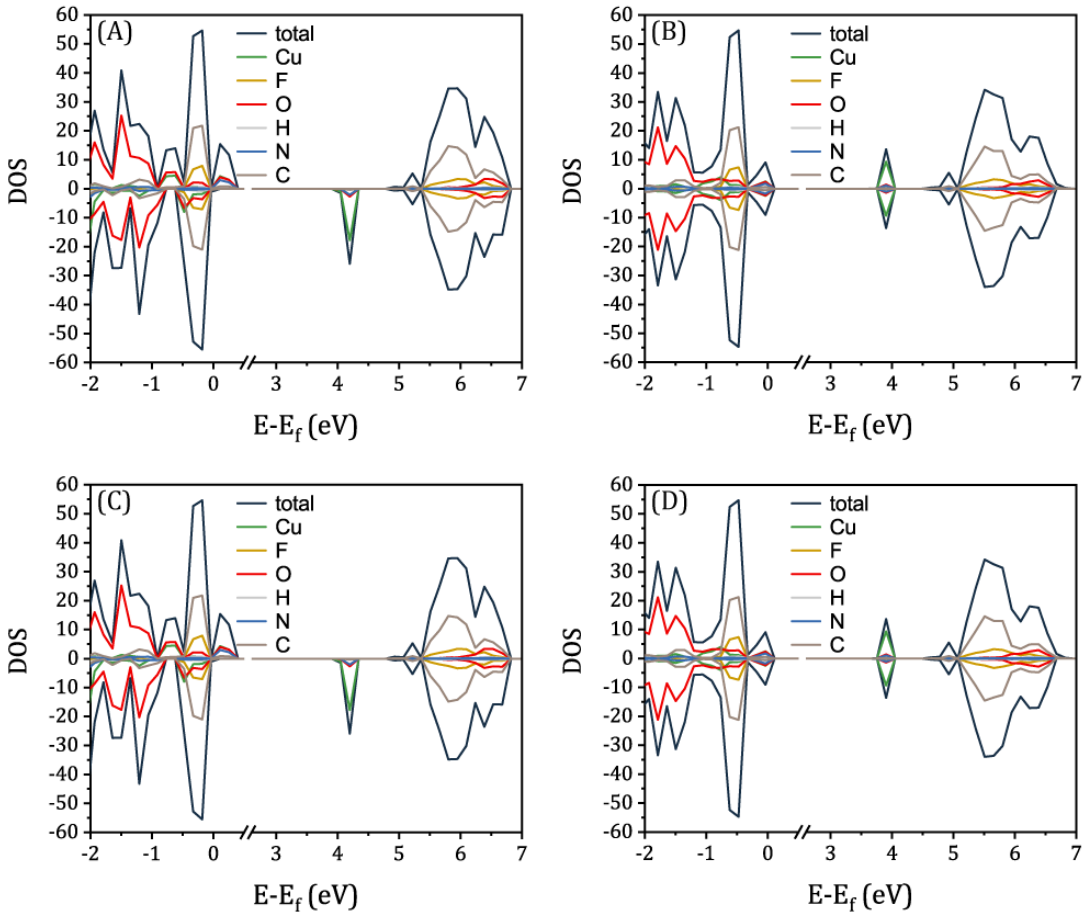

Figure S11: DFT calculations of L-F_5Phe-Cu and D-F_5Phe-Cu. (A) DOS of the ferromagnetic state of L-F_5Phe-Cu, showing states near the fermi energy, which originate mainly from the copper and ligands (nitrogen and oxygen atoms). **(B)** DOS of the antiferromagnetic state of L-F_5Phe-Cu, showing states near the fermi energy, which originate

mainly from the copper and ligands (nitrogen and oxygen atoms). **(C)** DOS of the ferromagnetic state of D-F_5Phe-Cu. **(D)** DOS of the antiferromagnetic state of D-F_5Phe-Cu.

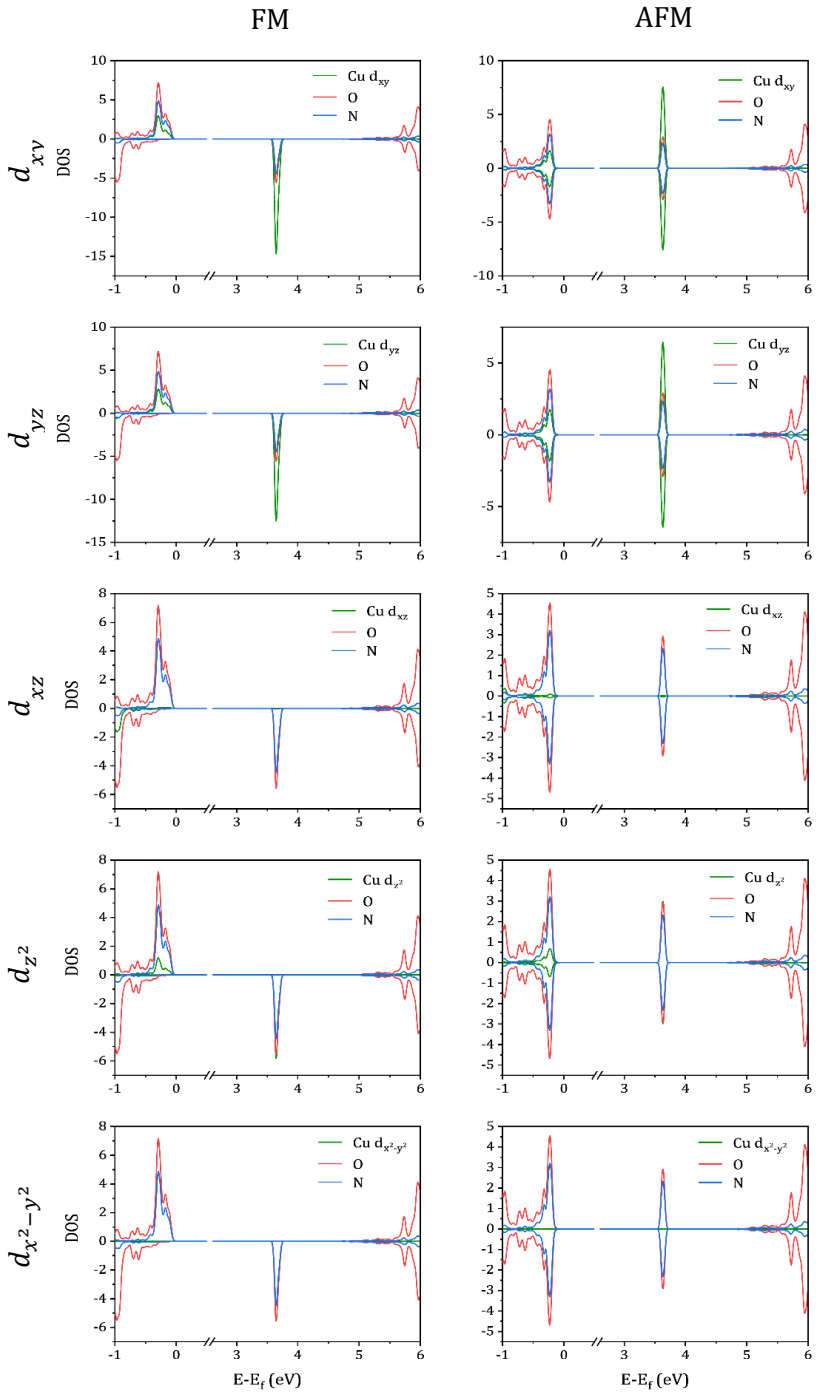

Figure S12: DFT calculations of the partial density of states (PDOS), for L-Phe-Cu FM (left) and AFM (right) states, projected on the different *d* orbitals of the Cu atom and the valence orbitals of O and N. It is readily observed that only d_{xy}, d_{yz}, and d_{z2} orbitals, which hybridize with valence orbitals of the adjacent O and N ligand atoms, contribute to the magnetism-related peak at ~3.6 eV. Positive (negative) values represent up (down) spin PDOS.